



Optimization of 5-arylidene barbiturates as potent, selective, reversible LSD1 inhibitors for the treatment of acute promyelocytic leukemia

Siyuan Xu^{b,e}, Chen Zhou^{a,c,e}, Rongfeng Liu^d, Qihua Zhu^c, Yungen Xu^{c,*}, Fei Lan^{b,*}, Xiaoming Zha^{a,*}

^a Department of Pharmaceutical Engineering, Department of Biomedical Engineering, Jiangsu Key Laboratory of Drug Screening, China Pharmaceutical University, Nanjing 210009, PR China

^b Liver Cancer Institute, Zhongshan Hospital, Fudan University, Key Laboratory of Carcinogenesis and Cancer Invasion, Ministry of Education, Key Laboratory of Epigenetics and Metabolism, Ministry of Science and Technology, and Institutes of Biomedical Sciences, Fudan University, Shanghai 200032, PR China

^c Department of Medicinal Chemistry, China Pharmaceutical University, Nanjing 210009, PR China

^d Shanghai ChemPartner Co. Ltd., Zhangjiang Hi-Tech Park, Shanghai 201203, PR China

ARTICLE INFO

Keywords:

LSD1
5-Arylidene barbiturate
Selective
Reversible
Leukemia

ABSTRACT

Histone lysine specific demethylase 1 (LSD1) is overexpressed in diverse hematologic disorders and recognized as a promising target for blood medicines. In this study, molecular docking-based virtual screening united with bioevaluation was utilized to identify novel skeleton of 5-arylidene barbiturate as small-molecule inhibitors of LSD1. Among the synthesized derivatives, **12a** exhibited reversible and potent inhibition ($IC_{50} = 0.41 \mu M$) and high selectivity over the MAO-A and MAO-B. Notably, **12a** strongly induced differentiation effect on acute promyelocytic leukemia NB4 cell line and distinctly escalated the methylation level on histone 3 lysine 4 (H3K4). Our findings indicate that 5-arylidene barbiturate may represent a new skeleton of LSD1 inhibitors and **12a** deserve as a promising agent for the further research.

1. Introduction

Lysine-specific demethylase 1 (LSD1), reported as the first histone demethylase, is a flavin-dependent amine oxidase enzyme, ushering in a new avenue in the chromatin remodeling.¹ As an element of co-repressor complexes, LSD1 facilitates target gene repression by removing mono- and dimethyl marks from lysine 4 of histone H3 (H3K4).² Nevertheless, LSD1-dependent demethylation of histone H3K9 results in the activation of androgen receptor (AR) target gene expression.³ However, the mechanisms that dominate this dual personality are poorly understood. LSD1 is a key histone demethylase that mediates the epigenetic landscape. A flurry of studies has provided sights into the particular biological roles of LSD1 and its potential relationships to pathological processes including carcinogenesis.^{4–6} LSD1 is considered to target cancerous cells rather than normal ones, which potentially empowers the alternative targeting of cancer.^{7,8} High-level LSD1 expression has been associated with an alarming risk of acute myeloid leukemia (AML), as well as prostate cancer, colon carcinoma, and

breast cancer.^{9–12} In addition to histones, LSD1 catalyzes the demethylation of p53, blocking p53 mutual effect with its coactivator 53BP1.¹³ Interestingly, elevated levels of LSD1 have a favorable effect on muscle recovery and regeneration after injuries, due to direct regulation of key myogenic transcription factor genes.¹⁴ Owing to abundant proof-of-concept studies forcefully back up its potential as a druggable target, obtaining selective and potent LSD1 inhibitors has emerged as a motivating and promptly evolving area of research.¹⁵

Up to now, plenty of LSD1 inhibitors with different scaffolds have been reported (Fig. 1).^{16–18} The most widely investigated LSD1 inhibitors were mechanism-based agents which demethylate histone lysine via redox reactions.¹⁹ Those agents are irreversible inhibitors acting as FAD competitor situating at the LSD1 active site.^{20–23} Two outstanding irreversible inhibitors,^{24–26} GSK2879552 (A) and RG-6016 (B) are currently undergoing advanced clinical trials for the treatment of AML (Fig. 1).^{27,28} Based on the TCPA scaffold, Hoang et al. developed a novel LSD1 inhibitor, CBB3001(C), which selectively inhibited teratocarcinoma and embryonic carcinoma cells that express SOX2 and

Abbreviations: LSD1, histone lysine specific demethylase 1; lysine 4 of histone H3, H3K4; MAO, monoamine oxidase; FAD, flavin adenine dinucleotide; VS, virtual screening; MST, microscale thermophoresis; ATRA, all-trans retinoic acid

* Corresponding authors.

E-mail addresses: xyg64@126.com (Y. Xu), fei_lan@fudan.edu.cn (F. Lan), xmzha@cpu.edu.cn (X. Zha).

^e These authors contributed equally to this work.

<https://doi.org/10.1016/j.bmc.2018.08.026>

Received 9 July 2018; Received in revised form 17 August 2018; Accepted 20 August 2018

0968-0896/ © 2018 Elsevier Ltd. All rights reserved.

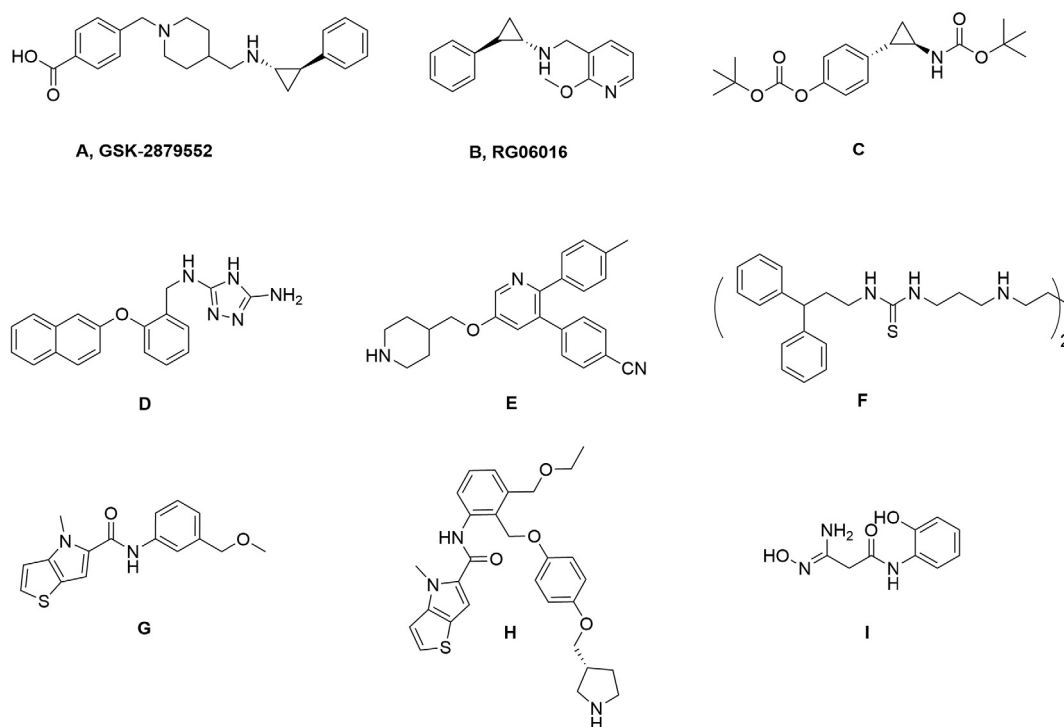


Fig. 1. Representative structures of reported LSD1 inhibitors.

OCT4.²⁹ Other than mechanism-based inhibitors, a limited number of potent reversible inhibitors of LSD1 have been developed, such as aminotriazoles (D),³⁰ pyridine containing compounds (E).³¹ Nowotarski and co-workers have reported a series of polyamine analogs (F) with thiourea moiety bearing potent inhibition to LSD1 activity.³² The SAR analysis suggested that the ability of these analogues to promote epigenetic changes was related to the length of the central chain. Very recently, Vianello *et al.* employed a high-throughput screening (HTS) strategy to get the compound **G** ($IC_{50} = 2.9 \mu M$) that upon further optimization yielded compound **H** with extremely high potency against LSD1 ($IC_{50} = 7.8 nM$).^{33,34} The reversible LSD1 inhibitors display some advantages over irreversible inhibitors, particularly in view of a safer metabolic profile.

The virtual screening (VS) has arisen as a powerful computational tool, which is commonly applied in drug discovery process.^{35,36} Apart from its convenience, this technique can help identify leading compounds with novel skeletons and provide structural clues for compound optimization.^{37,38} So far, several successful docking-based virtual screenings have been implemented with LSD1. Hazeldine *et al.* initiated VS to gain a variety of low molecular weight amidoximes as reversible LSD1 inhibitors of the most effective one (**I**) exhibited modest potency against LSD1 ($IC_{50} = 16.8 \mu M$).³⁹ Following our former success in this area,^{40–42} herein we report the successful acquisition of 5-arylidene barbiturate skeleton and design, synthesis and biological studies of a new series of LSD1 inhibitors. We initiated a docking-based VS to hunt for novel LSD1 inhibitors from the SPECS database and *in vitro* inhibition assaying campaign to identify potent and various lead compounds. We examined these hits by interaction analyses and selected two hits for structural optimization. Those two compounds were purchased for further bioactivity testing (See Table 1). Excitingly, these two molecules containing the same 5-arylidene barbiturates scaffold performed potent inhibitory activity in the micromolar range. Through analysing binding modes of the two compounds (Fig. 2), the hydrogen bond between Trp756 and hydrogen bond donor of ligand is critical to the interaction. The docking score of **XZ01** is lower than that of **XZ02**, which is consistent with their respective inhibitory activity. Chemical optimization was conducted to acquire more structural analogues on the basis

of the hit compounds. We introduced different aromatic rings bearing one or more hydrogen bond donors to the N1 position of the 5-arylidene barbiturates scaffold. What's more, benzene ring containing different substituents was introduced to the C5 position of the 5-arylidene barbiturates scaffold, aiming to achieve substituent diversity and explore the structure-activity relationships (SARs). Further experimental studies demonstrated that the derivative **12a** significantly inhibited acute promyelocytic leukemia cell proliferation. In conclusion, we report herein 5-arylidene barbiturates as novel potent, reversible and selective LSD1 inhibitors, and they can provide us with helpful structural clues to develop more powerful LSD1 inhibitors.

2. Results and discussion

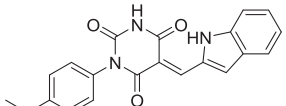
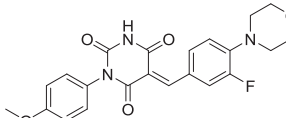
2.1. Predicted binding patterns of the two hit compounds

The two hits show similar binding poses predicted by molecular docking. As shown in Fig. 2, the binding poses of these two inhibitors are quite similar, and both can form the hydrogen bond interaction with Arg316, Ser287, Ser289. However, the C5 substitution of **XZ02** does not form H-bonding interactions with Trp756 which **XZ01** does have. Thus, according to the chemical structures of these two inhibitors, it may explain why **XZ01** showed three times inhibition activity than **XZ02**. It seems that the addition of a hydrogen donor group at C5 substitution, which formed a key H-bond with Trp756, may be beneficial for enhancing the inhibitory activity against LSD1.

2.2. Docking-based VS

In the present study, a docking-based VS strategy was used to identify promising hits. Indicated by the AUC values, the Glide SP scoring mode showed better discrimination power than the other two docking tools. In addition to the docking score rankings, visual inspection of the docking poses was used to assess binding mode and orientation. Taken together, this strategy identified a set of two hits. They were procured and screened in the LSD1 biochemical assay. Compound purity has been verified by vendors using nuclear magnetic

Table 1
Structures of two hit compounds and their inhibition rates (IC₅₀) to LSD1 *in vitro*.

Compound	Structures	SPECS ID	IC ₅₀ (μM) against LSD1	Glide Gscore (kJ/mol)
XZ01		AG-690/11763270	6.42	-11.05
XZ02		AH-487/41938748	18.2	-10.15

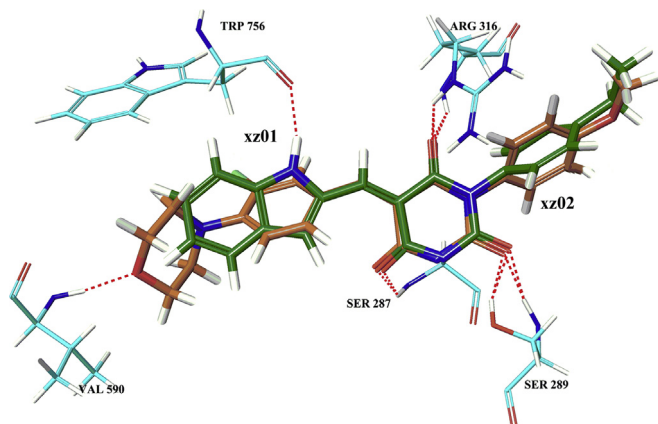


Fig. 2. The binding modes between XZ01, XZ02 and LSD1 (PDB id: 2Z5U), the hydrogen bonds interactions are highlighted using red dash line, XZ01 is represented as green sticks, XZ02 is represented as brown sticks, important residues are represented as blue sticks. (For interpretation of the references to colour in this figure legend, the reader is referred to the web version of this article.)

resonance (NMR) experiments.

2.3. Chemistry

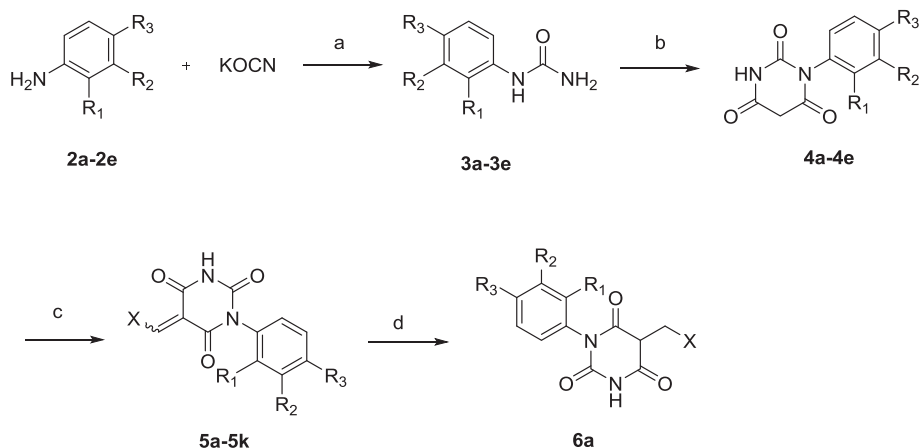
Compounds **5a-5k** could be readily synthesized using the routes described in [Scheme 1](#). The phenylurea derivatives were synthesized using the same method as described by Kurzer.⁴³ Treatment of aniline with sodium cyanate in the presence of glacial acetic acid in water gave compounds **3a-3e**, which then reacted with diethyl malonate in ethanol

solution of sodium alcohol under reflux, affording compounds **4a-4e**. With compounds **4a-4e** in hand, we next introduced different aldehyde substituents into the scaffold, aiming to achieve substituent diversity and explore the structure-activity relationships. The reactions between distinctive aldehydes and compounds **4a-4e** proceeded smoothly and efficiently under mild conditions, giving corresponding products **5a-5k** in good yields.

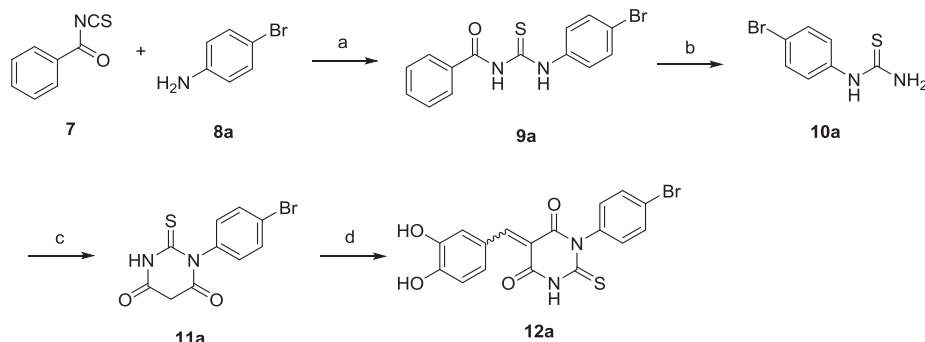
In order to further investigate the structure-activity relationships (SARs), we also performed additional structural modifications by replacing the oxygen atom at C2 position with sulphur atom and the reduction of the double bond at C5 position. The synthesis of compound **6a** could be completed in a single step, as shown in [Scheme 1](#). Compound **5k** was treated with sodium borohydride to afford the desired product **6a** in 70.8% yield. The remaining target molecule **12a** was synthesized as outlined in [Scheme 2](#). Treatment of **7** with the appropriate amiline **8a** in the presence of benzoyl chloride under reflux afforded the target molecule **9a**. **10a** was prepared from **9a** by treatment with preheated solution of aqueous sodium hydroxide (5%). Then **10a** was treated similarly to **3a-3e** and afforded the desired compound **12a** as shown in [Scheme 2](#).

2.4. Biochemical activity of the candidate compounds against LSD1 and SAR studies

All the compounds synthesized in this study were examined for their inhibitory effect on LSD1 activity *in vitro*. TCPA was chosen as a positive control. The results were summarized as [Tables 2-5](#). The results of compounds **5a-5f** against LSD1 were determined initially and shown in [Table 2](#). All the compounds exhibit moderate to good potency with IC₅₀ values ranging from 0.3 to 23 μM. Among them, compound **5c** shows the most potent activity to LSD1 (IC₅₀ = 0.3 μM), which is 12 times stronger than that of TCPA (IC₅₀ = 3.6 μM). During the SAR studies, we



Scheme 1. Synthesis of compounds **5a-k** and **6a**. Reagents and conditions: (a) AcOH, H₂O, rt, 2 h; (b) diethyl malonate, Na, ethanol, reflux; (c) appropriate aromatic aldehydes, ethanol, reflux, 2 h; (d) NaBH₄, rt.



Scheme 2. Synthesis of compound **12a**. Reagents and conditions: (a) acetone, reflux; (b) 5% NaOH, 85 °C; (c) diethyl malonate, Na, ethanol, reflux; (d) 3,4-dihydroxybenzaldehyde, ethanol, reflux, 2 h.

Table 2

Structures of compounds **5a-5f** and their inhibition data (IC_{50}) against LSD1 *in vitro*.

Compound	X	R ₁	R ₂	R ₃	IC_{50} (μ M)
5a		H	H	CH ₃	1.1
5b		CH ₃	H	H	4.4
5c		H	H	Br	0.3
5d		H	H	OCH ₃	3.1
5e		H	H	CN	1.2
5f		H	H	CH ₃	23
TCPA					3.6

Table 3

Structures of compounds **5g-5k** and their inhibition data (IC_{50}) against LSD1 *in vitro*.

Compound	R ₃	R ₄	R ₅	R ₆	R ₇	IC_{50} (μ M)
5g	Br	H	OCH ₃	OH	H	0.87
5h	Br	H	OH	OCH ₃	H	3.6
5i	Br	H	OCH ₃	OH	OCH ₃	0.55
5j	Br	OCH ₃	OCH ₃	OCH ₃	H	3.6
5k	Br	H	OCH ₃	OCH ₃	H	2.8
TCPA						3.6

Table 4

The structure of compound **12a** and the inhibition (IC_{50}) against LSD1 *in vitro*.

Compound	R ₃	X	IC_{50} (μ M)
12a	Br		0.41

Table 5

The structure of compound **6a** and the inhibition (IC_{50}) against LSD1 *in vitro*.

Compound	R ₃	X	IC_{50} (μ M)
6a	Br		> 75

found that the benzene ring substitution on the N1 was important for the inhibitory activity: the 4-Br substitution derivative compound **5c** was more potent than the other benzene ring substitution derivative compounds. Moreover, C5 substitution was also preferential: 3,4-dihydroxybenzyl substitution derivative compound **5c** (IC_{50} = 0.3 μ M) was more potent than 1H-indol-2-yl substitution derivative compound **5a** (IC_{50} = 1.11 μ M).

To determine the inhibitory effect of compounds against LSD1 at cellular level, acute promyeloid leukemia (APL) cell line NB4 was chosen.⁴⁴ NB4 is a cell line that has been used as a model to study APL. Its differentiation can be partially detected by a cell surface marker CD11b. Here, we used FACS to test how CD11b level change after the drug treatment to explore the drug's effect *in vivo*. **5a**, **5b**, **5c** and **5e** were submitted to *in vivo* differentiation assay. We used two reported irreversible LSD1 inhibitors, **TCPA** and **RN-1** (IC_{50} = 8 nM) as control.^{45,46} The results were summarized as Fig. 3. At the concentration of 5 μ M, our compounds **5a**, **5c** and **5e** perform strong differentiation effect on NB4 cells, among them **5c** and **5e** perform better and are stronger than **RN-1** (Fig. 10).

In view of the *in vitro* and *in vivo* inhibition assay of the first batch of compounds **5a-5f**, N1 substitution was locked as 4-Br. We also considered that the pyrocatechol part may be a false positive compound.

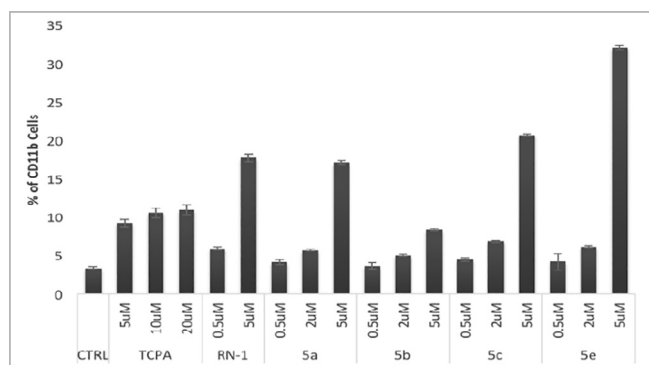


Fig. 3. The *in vivo* differentiation assay of 5a, 5b, 5c and 5e.

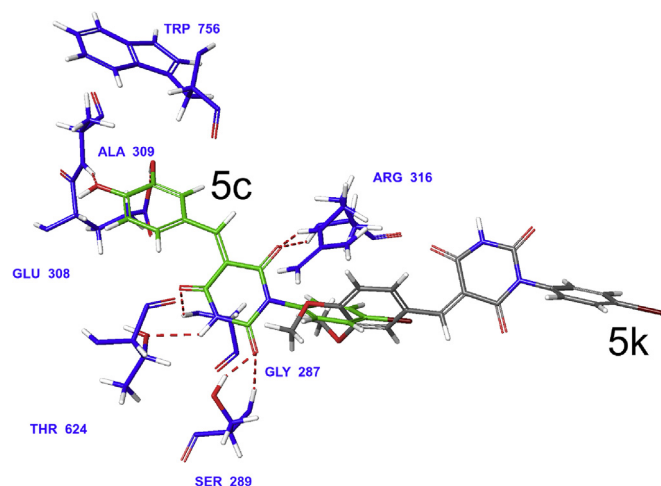


Fig. 4. The predicted binding modes between compounds 5c, 5k and LSD1 (PDB id: 2Z5U). Compounds 5c and 5k were highlighted in green, grey respectively. The hydrogen bonds interactions are highlighted using red dash line, important residues are represented as blue sticks. (For interpretation of the references to colour in this figure legend, the reader is referred to the web version of this article.)

Thus, we introduced different hydroxyl substituted benzene to the C5 position. Compounds 5g-5k were synthesized, and the results were shown in Table 3. Replacing the pyrocatechol scaffold with substituted benzene 5g-5k (Table 3) led to a lowered enzyme activity. 4-hydroxy-2,3-dimethoxybenzyl was better than the other substitutions. 5j which did not have phenol hydroxyl performed activity less than 3.0 μM. Those results indicated the significance of the phenolic hydroxyl group in retaining their activity. Furthermore, the predicted binding modes of compounds 5c and 5k in the active site of between LSD1 are displayed in Fig. 4. The compound 5c performed strong and various interactions with LSD1. Gly287, Ser 289, Arg316 and Thr624 formed hydrogen bonds with the 5-arylidene barbiturates scaffold. Besides, the OH of the C5 substituent also formed hydrogen bonds with surrounding Glu308 and Ala309 residues. In contrast, the compound 5k stretched in an opposite direction compared with 5c, which didn't show interactions with any key residues, such as Trp756 and Arg 316. The docking results may explain the difference of the activity.

Furthermore, the importance of barbituric scaffold of our compounds on LSD1 inhibitory activity was explored. We replaced the oxygen atom in C2 position with sulphur atom (Table 4). Benzyl pyrimidine-2,4,6-triones were also synthesized in order to evaluate the importance of the double bond in C5 position (Table 5). As can be seen from Table 4, substitution of the oxygen atom with a sulphur atom did not much affect the inhibition activity. 12a showed potent activity with

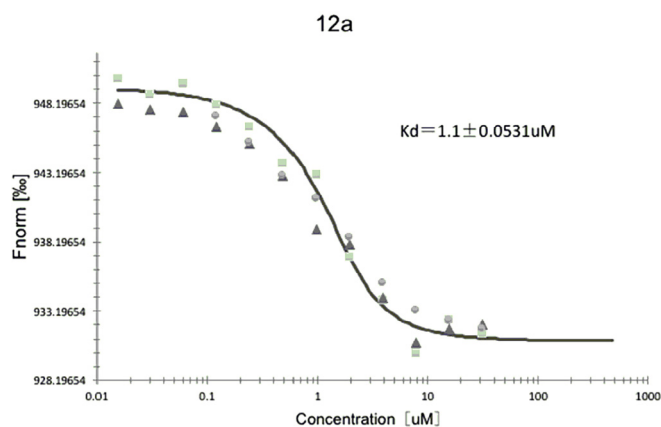


Fig. 5. K_d value for compounds 12a, obtained by microscale thermophoresis (MST) experiment.

IC₅₀ value of 0.41 μM. However, due to the reduction of the double bond in C5 position, compounds 6a did not exhibit LSD1 inhibitory effect, compared to the corresponding compound 5k. These findings indicate that the 5-arylidene barbituric scaffold is important to their inhibitory activity.

2.5. *In vitro* inhibition properties of compound 12a against the recombinant LSD1 and its homologues MAO-A and MAO-B.

Having identified compound 12a as a highly potent LSD1 inhibitor, we further determined the dissociation constant (K_d) of 12a by microscale thermophoresis (MST) experiment. MST assay shows the kinetic binding affinity between protein and molecules. The K_d value for compound 12a was 1.1 μM, indicating the robust binding affinity of 12a to LSD1 (Fig. 5).

To test the reversibility of compound 12a for LSD1, a dilution assay was used. Our analysis suggested that dilution of the LSD1/12a mixture by 100-fold resulted in the recovery of LSD1 activity, which indicated noncovalent interaction with the enzyme. The *in vitro* IC₅₀ of 12a toward LSD1 is 0.41 μM, the recombinant LSD1 was incubated with the compound at 4.1 μM for 1 h and then diluted 100-fold to test the LSD1 enzymatic activity. 98.19% of the enzymatic effect is restored, proving that 12a is a reversible LSD1 inhibitor (Fig. 6).

As LSD1 belongs to the monoamine oxidases (MAOs) family, the inhibitory effects of 12a to its homologues MAO-A and MAO-B were also examined. As shown in Fig. 7, 12a showed slight effect on MAO-A and MAO-B inhibitory activities. For MAO-A, the IC₅₀ of MAO-A is 72.52 μM, 175 times to its effect on LSD1 and for MAO-B, the IC₅₀ is out of the detection range indicating > 487-fold to LSD1. These findings

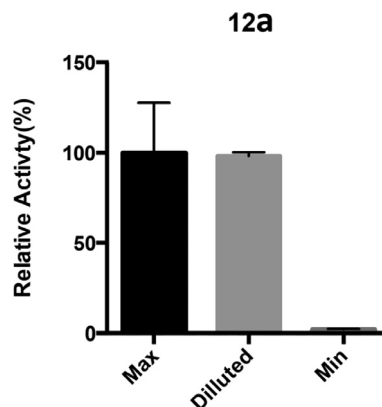


Fig. 6. The reversibility of compound 12a to LSD1 activity was determined by jump-dilution assay.

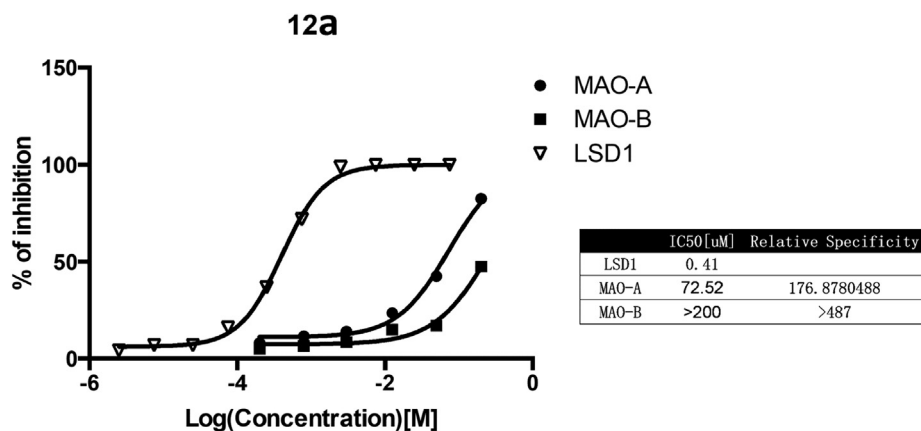


Fig. 7. In vitro inhibitory activities of compound 12a against LSD1 and its homologues MAO-A and MAO-B.

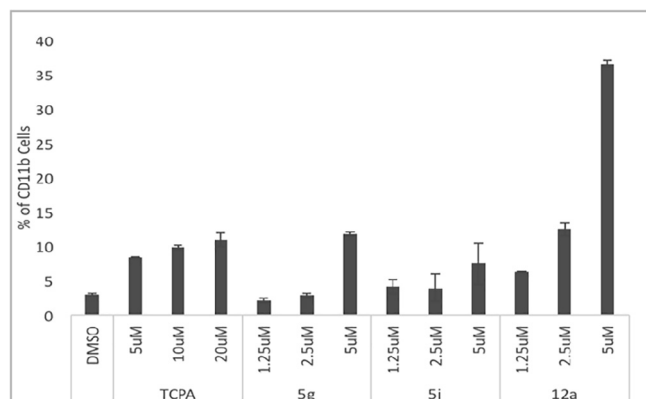


Fig. 8. The differentiation assay of 5g, 5i and 12a on NB4 cells.

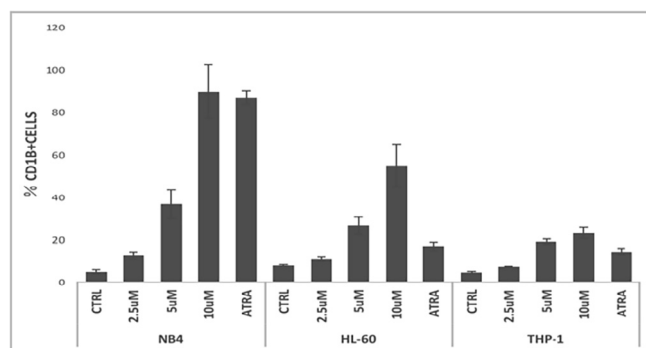


Fig. 9. The differentiation assay of 12a on NB4, HL-60 and THP-1 cell lines (ATRA in 0.1 μM concentration).

indicated a good selectivity of 12a toward LSD1 *in vitro*.

The differentiation assay result of the second batch of compounds 5g, 5i and 12a was summarized in Fig. 8. 12a showed strong differentiation effect on NB4 cells. At the concentrations of 2.5 μM and 5 μM, the differentiation rates were 12.5% and 36.6%, respectively. 5g

showed moderate differentiation effect, while 5i performed weak differentiation effect. Furthermore, we evaluated the differentiation effect of 12a on other leukemia cell lines such as HL-60 and THP-1 cell lines. As shown in Fig. 9, among three leukemia cell lines, 12a performed the most robust differentiation effects on NB4 cell lines with the differentiation rate of 89.7% at 10 μM comparing to 87% at 0.1 μM for ATRA as positive control.⁴⁷ (See Fig. 10).

To determine whether those compounds are cell active LSD1 inhibitors, the effects of six compounds on the methylation levels of LSD1 substrates H3K4 were analysed in human embryonic kidney 293 T cells (HEK 293 T). 293 T cells were treated for 24 h with vehicle or 2.5, 5, or 10 μM of compound 12a for 24 h. We particularly selected the H3K4me1 and H3K4me2 marks. The results are summarized in Fig. 11. Among these compounds assayed, 12a displayed the most potent improvement of methylation on H3K4me1 and H3K4me2. Moreover, 12a could elevate the methylation on H3K4me2 at 2.5 μM and particularly significantly improved the methylation on H3K4me1 at 10 μM, which may explain, compared to other compounds, why it owned more potent effect of differentiation inducing. These results validated that the compound 12a can decrease LSD1 activity at the cellular level.

3. Conclusion

In this study, docking-based VS combined with bioassays was employed to identify two hits compounds bearing skeleton of 5-arylidene barbiturate as LSD1 inhibitors in a micromolar range. After analysing their binding modes with LSD1, optimizations of the hits were carried out and 13 derivatives were synthesized. Among them, 12a, the most potent compound (IC₅₀ = 0.41 μM) displayed as a selective and reversible LSD1 inhibitor and exhibited strong differentiation inducing effect on LSD1-overexpressed acute promyelocytic leukemia NB4 cells. Furthermore, 12a also demonstrated potent improvement of methylation and dimethylation of H3K4. Taken together, 5-arylidene barbiturates represent a new class of potent, selective and reversible LSD1 inhibitors and 12a deserves a lead compound for the future development of reversible LSD1 inhibitors.

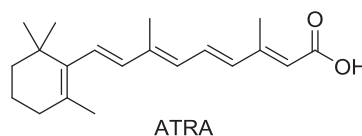
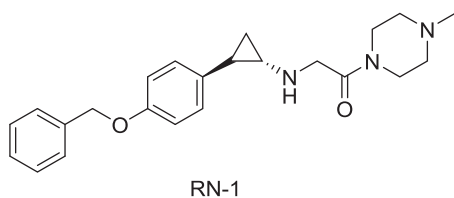


Fig. 10. Chemical structures of control compounds, RN-1 and ATRA.

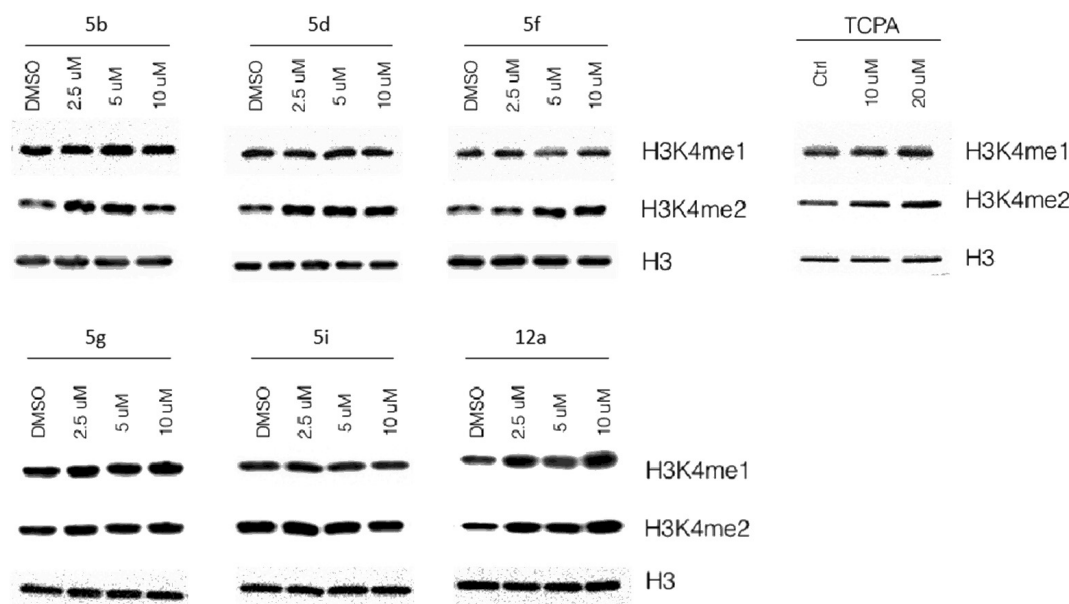


Fig. 11. Effect of six compounds including **12a** on histone methylation.

4. Experimental section

4.1. General

Reagents and solvents were purchased from commercial sources and were used without further purification. NMR spectra were recorded on a Bruker AMX-300 (^1H at 300 MHz, ^{13}C at 75 MHz) spectrometer. Proton and carbon NMR chemical shifts are reported as values in ppm with residual protic solvent as standard. All reagents were used as supplied by the manufacturer. Analytical thin-layer chromatography (TLC) was performed on pre-coated glass backed plates (Merck Kieselgel F₂₅₄).

4.1.1. General procedure for the synthesis of substituted phenylureas (**3a-3e**)

The phenylurea derivatives were synthesized according to the method described by Kurzer. Briefly, the aniline (0.05 mol) was dissolved in glacial acetic acid (24 mL) and water (48 mL). To this solution, was slowly added under stirring the sodium cyanate (0.1 mol) dissolved in water (45 mL). When a white precipitate appeared, the solution was stirred for 1 additional hour, then it was allowed to stand at rt for 2–3 h. The solution was cooled to 0 °C before filtration. The resulting phenylurea was washed with cold water, and was used without any further purification.

4.1.2. General procedure for the synthesis of pyrimidine-2,4,6-triones (**4a-4e**)

Sodium (20 mmol) was added portionwise to ethanol (60 mL) at rt. After dissolution of the sodium, urea (10 mmol) and diethyl malonate (10 mmol) were added sequentially each in one portion to the solution with stirring at rt and then heated at reflux for 5 h. Solvent was concentrated under reduced pressure and the remaining residue was dissolved in 1 M sodium hydroxide solution (20 mL). The aqueous layer was washed with ethyl acetate (2 × 20 mL) and then acidified (pH = 1) with 1 M aqueous hydrochloric acid solution and the resulting precipitate was filtered. The isolated solid material was recrystallized from methanol to give **4a-4e** as colorless solids.

4.1.3. General procedure for the synthesis of benzylidene pyrimidine-2,4,6-triones (**5a-5k**)

Appropriate aldehyde (5 mmol) was added in one portion to a

solution of **4a-4e** (5 mmol) in ethanol (20 mL) at rt. The reaction mixture was heated at reflux for 1 h. The reaction mixture was cooled down and the resulting precipitate was filtered and recrystallized from water to give **5a-5k** as yellow solids as a 1:1 mixture of geometrical isomers (*E/Z*).

4.1.3.1. (*E/Z*)-5-((1*H*-indol-2-yl)methylene)-1-(*p*-tolyl)pyrimidine-2,4,6-(1*H*,3*H*,5*H*)-trione (5a**).** Yellow solid, yield: 90%, M. p. > 250 °C. IR (KBr): 3030.2, 1734.0, 1689.6, 1645.3, 1546.9, 1328.9, 1130.3, 871.8, 750.3 cm^{-1} . ^1H NMR (300 MHz, DMSO- d_6) δ 12.47 (s, 1H, indole -NH-), 12.11 (s, 1H, indole -NH-), 11.81 (s, 1H, -NH-), 11.68 (s, 1H, -NH-), 8.40 (s, 1H, -CH-), 8.34 (s, 1H, -CH-), 7.73–7.72 (m, 6H, ArH), 7.69–7.08 (m, 12H, ArH), 2.38 (s, 3H, -CH₃-), 2.37 (s, 3H, -CH₃-). ^{13}C NMR (75 MHz, DMSO- d_6) δ 163.33, 162.74, 150.22, 150.20, 142.36, 141.98, 139.95, 139.72, 137.79, 137.58, 132.88, 132.66, 132.16, 131.97, 129.35, 129.23, 128.88, 128.71, 127.75, 127.69, 127.59, 127.44, 122.52, 122.38, 122.01, 121.50, 121.06, 121.02, 114.48, 113.64, 113.42, 112.07, 20.70. HRMS m/z ($[\text{M} + \text{H}]^+$) calcd for C₂₀H₁₆N₃O₃: 346.1186; found: 346.1188.

4.1.3.2. (*E/Z*)-5-((1*H*-indol-2-yl)methylene)-1-(*o*-tolyl)pyrimidine-2,4,6-(1*H*,3*H*,5*H*)-trione (5b**).** Yellow solid, yield: 82.0%, M. p. > 250 °C. IR (KBr): 3066.8, 1726.3, 1683.9, 1651.1, 1533.4, 1338.6, 1107.1, 829.7, 718.7 cm^{-1} . ^1H NMR (300 MHz, DMSO- d_6) δ 12.47 (s, 1H, indole -NH-), 12.08 (s, 1H, indole -NH-), 11.88 (s, 1H, -NH-), 11.76 (s, 1H, -NH-), 8.43 (s, 1H, -CH-), 8.36 (s, 1H, -CH-), 7.75–7.70 (m, 6H, ArH), 7.43–7.29 (m, 10H, ArH), 7.17–7.08 (m, 2H, ArH), 2.14 (s, 3H, -CH₃-), 2.11 (s, 3H, -CH₃-). ^{13}C NMR (75 MHz, DMSO- d_6) δ 163.36, 163.13, 162.90, 162.78, 149.71, 142.59, 142.39, 140.10, 139.83, 136.18, 136.02, 134.54, 134.33, 132.18, 131.98, 130.43, 130.32, 129.26, 129.13, 128.65, 128.55, 127.86, 127.81, 127.61, 127.44, 126.64, 126.49, 122.58, 122.42, 122.38, 121.77, 121.07, 113.74, 113.47, 111.97, 111.65, 16.98, 16.97. HRMS (ESI): m/z $[\text{M} + \text{H}]^+$ calcd for C₂₀H₁₅N₃O₃: 346.1186; found: 346.1194.

4.1.3.3. (*E/Z*)-1-(4-bromophenyl)-5-(3,4-dihydroxybenzylidene)pyrimidine-2,4,6-(1*H*,3*H*,5*H*)-trione (5c**).** Yellow solid, yield: 74.3%, M. p. > 250 °C. IR (KBr): 3176.7, 1716.6, 1683.9, 1673.8, 1509.2, 1300.6, 1169.4, 827.5, 785.9 cm^{-1} . ^1H NMR (300 MHz, DMSO- d_6) δ 11.57 (s, 1H, -NH), 11.46 (s, 1H, -NH), 10.42 (s, 2H, -OH), 9.50 (s, 2H, -OH), 8.22–8.15 (m, 2H, -CH-, 2H, ArH), 7.68–7.56 (m, 6H, ArH), 7.30

(d, $J = 8.1$ Hz, 4H, ArH), 6.86 (s, 1H, ArH), 6.83 (s, 1H, ArH). ^{13}C NMR (75 MHz, DMSO- d_6) δ 163.80, 163.23, 161.66, 161.42, 156.82, 156.58, 152.66, 152.56, 150.12, 150.05, 144.91, 135.15, 134.97, 131.98, 131.76, 131.74, 131.60, 131.41, 124.32, 124.19, 121.33, 121.04, 115.43, 113.96, 113.65. HRMS m/z : $([\text{M} + \text{H}]^+)$ calcd for $\text{C}_{17}\text{H}_{11}\text{BrN}_2\text{O}_5$: 402.9924; found: 402.9931.

4.1.3.4. (E/Z)-5-(3,4-dihydroxybenzylidene)-1-(4-methoxyphenyl)pyrimidine-2,4,6(1H,3H,5H)-trione (5d). Yellow solid, yield: 74.6%, M. p. > 250 °C. IR (KBr): 3176.7, 1722.4, 1685.8, 1662.6, 1537.3, 1317.4, 1138.0, 825.5, 779.2 cm^{-1} . ^1H NMR (300 MHz, DMSO- d_6) δ 11.51 (s, 1H, -NH-), 11.40 (s, 1H, -NH-), 10.39 (s, 2H, -OH), 9.51 (s, 2H, -OH), 8.25–8.15 (m, 2H, -CH-, 2H, ArH), 7.67–7.56 (m, 2H, ArH), 7.25–7.20 (m, 4H, ArH), 7.02–6.98 (m, 4H, ArH), 6.88–6.83 (m, 2H, ArH), 3.80 (s, 6H, -OCH₃). ^{13}C NMR (75 MHz, DMSO- d_6) δ 164.02, 163.20, 161.93, 161.41, 158.84, 158.77, 156.69, 156.32, 152.50, 152.38, 150.43, 150.37, 144.85, 144.83, 140.50, 132.00, 131.30, 130.18, 129.99, 128.18, 127.95, 124.32, 124.18, 121.20, 120.88, 115.36, 114.06, 113.93, 113.87, 113.73, 55.31, 55.26. HRMS m/z : $([\text{M} + \text{H}]^+)$ calcd for $\text{C}_{18}\text{H}_{14}\text{N}_2\text{O}_6$: 355.0925; found: 355.0925.

4.1.3.5. (E/Z)-4-(5-(3,4-dihydroxybenzylidene)-2,4,6-trioxotetrahydropyrimidin-1(2H)-yl)benzonitrile (5e). Yellow solid, yield: 87.3%, M. p. 229 ~ 230 °C. IR (KBr): 3184.5, 1734.3, 1697.4, 1681.9, 1506.4, 1338.6, 1136.1, 846.7, 785.9 cm^{-1} . ^1H NMR (300 MHz, DMSO- d_6) δ 11.64 (s, 1H, -NH-), 11.53 (s, 1H, -NH-), 10.42 (s, 2H, -OH), 9.51 (s, 2H, -OH), 8.25–8.16 (m, 2H, -CH-, 2H, ArH), 7.98–7.95 (m, 4H, ArH), 7.67–7.56 (m, 6H, ArH), 6.89 (s, 1H, ArH), 6.82 (s, 1H, ArH). ^{13}C NMR (75 MHz, DMSO- d_6) δ 163.65, 163.21, 161.52, 161.39, 156.84, 156.74, 152.75, 152.65, 149.93, 149.84, 144.88, 140.17, 140.08, 132.88, 132.84, 132.20, 131.55, 130.74, 130.54, 124.22, 124.10, 121.26, 120.90, 118.45, 115.42, 113.76, 113.44, 111.08. HRMS m/z : $([\text{M} + \text{H}]^+)$ calcd for $\text{C}_{18}\text{H}_{11}\text{N}_3\text{O}_5$: 350.0771; found: 350.0774.

4.1.3.6. (E/Z)-5-(3-hydroxybenzylidene)-1-(p-tolyl)pyrimidine-2,4,6(1H,3H,5H)-trione (5f). Yellow solid, yield: 70.1%, M. p. 249–250 °C. IR (KBr): 3118.9, 1732.1, 1670.4, 1635.6, 1556.5, 1319.3, 1161.2, 894.9, 790.8 cm^{-1} . ^1H NMR (300 MHz, DMSO- d_6) δ 11.68 (s, 1H, -NH), 11.54 (s, 1H, -NH), 9.71 (s, 1H, -OH), 9.65 (s, 1H, -OH), 8.28 (s, 1H, -CH-), 8.21 (s, 1H, -CH-), 7.63 (s, 2H, ArH), 7.45–7.17 (m, 12H, ArH), 6.97–6.91 (m, 2H, ArH), 2.36 (s, 6H, -CH₃). ^{13}C NMR (75 MHz, DMSO- d_6) δ 163.19, 162.53, 161.09, 160.74, 156.82, 156.79, 155.51, 155.22, 150.26, 150.21, 137.61, 137.59, 133.77, 133.63, 132.83, 132.57, 129.21, 129.18, 129.10, 129.05, 128.81, 128.66, 125.02, 124.65, 119.69, 119.60, 119.27, 119.06, 119.00, 118.93, 20.71, 20.68. HRMS m/z : $([\text{M} + \text{H}]^+)$ calcd for $\text{C}_{18}\text{H}_{14}\text{N}_2\text{O}_4$: 323.1026; found: 323.1034.

4.1.3.7. (E/Z)-1-(4-bromophenyl)-5-(4-hydroxy-3-methoxybenzylidene)pyrimidine-2,4,6(1H,3H,5H)-trione (5g). Yellow solid, yield: 69.5%, M. p. > 250 °C. IR (KBr): 3434.5, 1725.5, 1696.9, 1617.6, 1488.6, 1338.7, 1168.2, 825.7, 790.4 cm^{-1} . ^1H NMR (300 MHz, DMSO- d_6) δ 11.62 (s, 1H, -NH-), 11.51 (s, 1H, -NH-), 10.59 (s, 1H, -OH), 10.56 (s, 1H, -OH), 8.47 (s, 1H, -CH-), 8.34 (s, 1H, -CH-), 8.25 (s, 1H, ArH), 8.24 (s, 1H, ArH), 7.91–7.79 (m, 2H, ArH), 7.69–7.66 (m, 4H, ArH), 7.33–7.29 (m, 4H, ArH), 6.93–6.87 (m, 2H, ArH), 3.84 (s, 3H, -OCH₃), 3.76 (s, 3H, -OCH₃). ^{13}C NMR (75 MHz, DMSO- d_6) δ 166.63, 166.59, 163.15, 161.62, 156.65, 156.37, 153.20, 151.33, 150.10, 149.99, 146.94, 134.90, 134.31, 132.62, 132.25, 131.83, 131.53, 131.35, 131.16, 124.18, 124.04, 121.45, 121.34, 118.46, 117.85, 115.32, 115.32, 114.23, 114.14, 55.63, 55.49. HRMS m/z : $([\text{M} + \text{H}]^+)$ calcd for $\text{C}_{18}\text{H}_{13}\text{BrN}_2\text{O}_5$: 417.0081; found: 417.0089.

4.1.3.8. (E/Z)-1-(4-bromophenyl)-5-(3-hydroxy-4-methoxybenzylidene)pyrimidine-2,4,6(1H,3H,5H)-trione (5h). Yellow solid, yield: 78.4%, M. p. > 250 °C. IR (KBr): 3510.7, 1736.4, 1696.6, 1664.0, 1501.1,

1335.9, 1147.5, 807.9, 789.1 cm^{-1} . ^1H NMR (300 MHz, DMSO- d_6) δ 11.63 (s, 1H, -NH), 11.52 (s, 1H, -NH), 9.45 (s, 1H, -OH), 9.43 (s, 1H, -OH), 8.26 (s, 1H, -CH-), 8.18 (s, 1H, -CH-), 8.14 (s, 2H, ArH), 7.75–7.64 (m, 6H, ArH), 7.33–7.28 (m, 4H, ArH), 7.10–7.03 (m, 2H, ArH), 3.90 (s, 3H, -OCH₃), 3.87 (s, 3H, -OCH₃). ^{13}C NMR (75 MHz, DMSO- d_6) δ 163.58, 163.02, 161.49, 161.29, 156.26, 156.06, 153.07, 153.00, 150.07, 149.99, 145.81, 145.78, 135.06, 134.86, 131.72, 131.52, 131.34, 130.99, 130.38, 125.37, 125.25, 121.34, 120.32, 120.00, 115.31, 115.03, 111.29, 111.26, 55.77, 55.73. HRMS m/z : $([\text{M} + \text{H}]^+)$ calcd for $\text{C}_{18}\text{H}_{13}\text{BrN}_2\text{O}_5$: 417.0081; found: 417.0086.

4.1.3.9. (E/Z)-1-(4-bromophenyl)-5-(4-hydroxy-2,3-dimethoxybenzylidene)pyrimidine-2,4,6(1H,3H,5H)-trione (5i). Yellow solid, yield: 88.1%, M. p. > 250 °C. IR (KBr): 3408.8, 1726.9, 1682.6, 1667.0, 1489.4, 1307.3, 1162.1, 832.3, 788.3 cm^{-1} . ^1H NMR (300 MHz, DMSO- d_6) δ 11.65 (s, 1H, -NH), 11.54 (s, 1H, -NH), 10.06 (s, 2H, -OH), 8.38 (s, 1H, -CH-), 8.28 (s, 1H, -CH-), 8.01 (s, 2H, ArH), 7.94 (s, 2H, ArH), 7.68 (d, $J = 8.2$ Hz, 4H, ArH), 7.34–7.30 (m, 4H, ArH), 3.84 (s, 6H, -OCH₃), 3.78 (s, 6H, -OCH₃). ^{13}C NMR (75 MHz, DMSO- d_6) δ 163.72, 163.16, 161.72, 161.63, 157.03, 156.80, 150.10, 149.97, 147.08, 142.72, 142.62, 135.09, 134.94, 131.80, 131.73, 131.55, 131.36, 122.78, 122.69, 121.35, 114.48, 114.32, 114.06, 113.86, 56.09, 56.01. HRMS m/z : $([\text{M} + \text{H}]^+)$ calcd for $\text{C}_{19}\text{H}_{15}\text{BrN}_2\text{O}_6$: 447.0186; found: 447.0189.

4.1.3.10. (E/Z)-1-(4-bromophenyl)-5-(2,3,4-trimethoxybenzylidene)pyrimidine-2,4,6(1H,3H,5H)-trione (5j). Yellow solid, yield: 89.1%, M. p. > 250 °C. IR (KBr): 3448.1, 1735.2, 1697.5, 1664.6, 1493.9, 1377.3, 1100.1, 830.4, 789.8 cm^{-1} . ^1H NMR (300 MHz, DMSO- d_6) δ 11.66 (s, 1H, -NH), 11.51 (s, 1H, -NH), 8.58 (s, 1H, -CH-), 8.54 (s, 1H, -CH-), 8.35 (d, $J = 9.2$ Hz, 1H, ArH), 8.15 (d, $J = 9.2$ Hz, 1H, ArH), 7.69–7.65 (m, 4H, ArH), 7.31–7.28 (m, 4H, ArH), 6.95 (d, $J = 9.6$ Hz, 1H, ArH), 6.85 (d, $J = 9.3$ Hz, 1H, ArH), 3.93 (s, 3H, -OCH₃), 3.91 (s, 3H, -OCH₃), 3.88 (s, 3H, -OCH₃), 3.87 (s, 3H, -OCH₃), 3.78 (s, 3H, -OCH₃), 3.76 (s, 3H, -OCH₃). ^{13}C NMR (75 MHz, DMSO- d_6) δ 163.42, 162.81, 161.19, 161.05, 158.10, 158.05, 154.95, 154.90, 150.11, 150.00, 149.95, 149.74, 140.65, 140.58, 134.94, 134.73, 131.68, 131.44, 131.33, 129.38, 129.24, 121.37, 121.31, 118.91, 118.81, 116.83, 116.68, 107.23, 107.07, 61.98, 60.48, 56.26, 56.21. HRMS m/z : $([\text{M} + \text{H}]^+)$ calcd for $\text{C}_{20}\text{H}_{17}\text{BrN}_2\text{O}_6$: 461.0341; found: 461.0347.

4.1.3.11. (E/Z)-1-(4-bromophenyl)-5-(3,4-dimethoxybenzylidene)pyrimidine-2,4,6(1H,3H,5H)-trione (5k). Yellow solid, yield: 80.5%, M. p. > 250 °C. IR (KBr): 3447.1, 1735.2, 1691.1, 1667.1, 1504.4, 1338.2, 1149.6, 829.2, 792.1 cm^{-1} . ^1H NMR (300 MHz, DMSO- d_6) δ 11.66 (s, 1H, -NH), 11.56 (s, 1H, -NH), 8.39 (s, 1H, -CH-), 8.37 (s, 1H, -CH-), 8.29 (s, 1H, ArH), 8.19 (s, 1H, ArH), 7.96–7.90 (m, 2H, ArH), 7.67 (d, $J = 7.9$ Hz, 4H, ArH), 7.33–7.28 (m, 4H, ArH), 7.15–7.08 (m, 2H, ArH), 3.90 (s, 3H, -OCH₃), 3.87 (s, 3H, -OCH₃), 3.83 (s, 3H, -OCH₃), 3.74 (s, 3H, -OCH₃). ^{13}C NMR (75 MHz, DMSO- d_6) δ 163.55, 162.97, 161.59, 161.53, 156.16, 155.89, 153.72, 153.69, 150.08, 149.96, 147.77, 135.04, 134.84, 131.76, 131.49, 131.33, 125.25, 125.13, 121.37, 117.03, 116.63, 115.56, 115.51, 111.08, 111.05, 55.84, 55.82, 55.52, 55.40. HRMS m/z : $([\text{M} + \text{H}]^+)$ calcd for $\text{C}_{19}\text{H}_{15}\text{BrN}_2\text{O}_5$: 431.0237; found: 431.024.

4.1.4. Synthesis of 1-(4-bromophenyl)-5-(3,4-dimethoxybenzyl)pyrimidine-2,4,6(1H,3H,5H)-trione (6a)

Sodium borohydride (3 mmol) was added in one portion to a stirred solution of **5k** (2 mmol) in ethanol (20 mL) at rt. The reaction mixture was stirred at rt for 1 h. The reaction mixture was concentrated under reduced pressure and the remaining residue was dissolved in water and acidified with aqueous hydrochloric acid solution (pH = 1). The resulting precipitate was filtered and recrystallized from water to give **6a** as white solids, yield: 70.8%, M. p. 186–188 °C. IR (KBr): 3231.1, 1701.3, 1516.9, 1321.9, 823.9, 824.6, 764.5 cm^{-1} . ^1H NMR (300 MHz, DMSO- d_6) δ 11.59 (s, 1H, -NH-), 7.66 (d, $J = 8.0$ Hz, 2H, ArH),

6.98–6.88 (m, 3H, ArH), 6.69–6.62 (m, 2H, ArH), 3.99 (s, 1H, CH), 3.73 (s, 3H, $-\text{OCH}_3$), 3.70 (s, 3H, $-\text{OCH}_3$), 3.30 (d, $J = 3.3$ Hz, 2H, $-\text{CH}_2-$). ^{13}C NMR (75 MHz, $\text{DMSO}-d_6$) δ 169.25, 169.16, 150.34, 148.34, 147.77, 134.05, 131.90, 130.85, 129.01, 121.52, 120.97, 112.59, 111.63, 55.42, 55.28, 50.63, 34.95. HRMS m/z : $([\text{M} + \text{Na}]^+)$ calcd for $\text{C}_{19}\text{H}_{17}\text{BrN}_2\text{O}_5$: 455.0213; found: 455.021.

4.1.5. Synthesis of *N*-substituted thioureas (**10a**)

Benzoyl chloride (0.01 mol) was added over 5 min to a freshly prepared solution of ammonium isothiocyanate (0.012 mol) in reagent grade acetone and the mixture was heated under reflux for about 15 min. Heating was stopped and appropriate aniline in acetone was added. The mixture was heated under reflux for 30 min and then poured on to crushed ice. The resulting solid was collected, washed with water, followed by cold mixture of water and methanol (1:1). Suitably substituted benzoylthioureas were added to a preheated solution of aqueous sodium hydroxide (5%) and stirred. The mixture was then poured into crushed ice containing hydrochloric acid (5%). The benzoic acid separated was removed by treating the reaction mixture with sodium carbonate. The product was collected, washed with water and dried to afford **10a**.

4.1.6. Synthesis of thioxopyrimidine-4,6-diones (**11a**)

Sodium (20 mmol) was added portionwise to ethanol (60 mL) at rt. After dissolution of the sodium, urea (10 mmol) and diethyl malonate (10 mmol) were added sequentially each in one portion to the solution with stirring at rt and then heated at reflux for 5 h. Solvent was concentrated under reduced pressure and the remaining residue was dissolved in 1 M sodium hydroxide solution (20 mL). The aqueous layer was washed with ethyl acetate (2×20 mL) and then acidified (pH 1) with 1 M aqueous hydrochloric acid solution and the resulting precipitate was filtered. The isolated solid material was recrystallized from methanol to give **11a** as colorless solid.

4.1.7. Synthesis of (*E/Z*)-1-(4-bromophenyl)-5-(3,4-dihydroxybenzylidene)-6-thioxodihydropyrimidine-2,4(1H,3H)-dione (**12a**)

3,4-Dihydroxybenzaldehyde (5 mmol) was added in one portion to a solution of **11a** (5 mmol) in ethanol (20 mL) at rt. The reaction mixture was heated at reflux for 1 h. The reaction mixture was cooled down and the resulting precipitate was filtered and recrystallized from water to give **12a** as yellow solids as a 1:1 mixture of geometrical isomers (*E/Z*). Yellow solid, yield: 75.9%, M. p. > 250 °C. IR (KBr): 3394.4, 3269.7, 1695.9, 1660.8, 1543.9, 1367.7, 1175.4, 784.2 cm^{-1} . ^1H NMR (300 MHz, $\text{DMSO}-d_6$) δ 12.16 (s, 2H, $-\text{NH}-$), 10.59 (s, 2H, $-\text{OH}$), 9.59 (s, 2H, $-\text{OH}$), 8.28 (s, 2H, $-\text{CH}-$), 8.22 (s, 2H, ArH), 7.67–7.64 (m, 6H, ArH), 7.28–7.26 (m, 4H, ArH), 6.86 (d, $J = 8.4$ Hz, 2H, ArH). ^{13}C NMR (75 MHz, $\text{DMSO}-d_6$) δ 179.12, 162.69, 161.40, 160.05, 159.05, 157.95, 157.58, 153.50, 153.40, 145.02, 138.87, 138.79, 132.94, 132.32, 131.78, 131.57, 131.41, 124.53, 124.37, 121.40, 121.22, 120.99, 115.56, 114.10, 113.79. HRMS m/z : $([\text{M} + \text{H}]^+)$ calcd for $\text{C}_{17}\text{H}_{11}\text{BrN}_2\text{O}_4\text{S}$: 418.9696; found: 418.9683.

4.2. Preparation of protein structure

The crystal structure of LSD1 resolved with the FAD cofactor was retrieved from the Protein Data Bank (PDB id: 2Z5U). The water molecules were removed. The remaining protein structure was prepared using the Protein Preparation Wizard module (Schrödinger, LLC, New York, NY, 2013). In short, the hydrogen atoms were added to the complexes. The module automatically optimize hydroxyl, Asn, Gln, and His states using ProtAssign. Finally, the complex was submitted to a restrained minimization using the OPLS2005 force field until the root-mean-square deviation reached a maximum value of 0.2 Å. The other parameters were set as default.

4.3. Preparing the ligand database

A Specs database containing 208 715 compounds was used as a ligand source. The three-dimensional conformations of the ligands were generated with LigPrep in Schrödinger, and their protonation states were determined at a target pH 7.0 ± 2.0 with Epik.

4.4. Glide docking procedure

The Glide program was used to generate the grid file. The bounding box of size $10 \text{ \AA} \times 10 \text{ \AA} \times 10 \text{ \AA}$ was centered on the FAD. Docking was performed using Glide software (Glide, version 5.9; Schrödinger, LLC: New York, NY, 2013) with standard precision (SP) mode. Top-ranked compounds with docking scores lower than -12.0 kJ/mol were retained and filtered by the Lipinski rule. Two compounds that are available from Specs were purchased and submitted to biological experimental.

4.5. GOLD docking procedure

Molecule docking experiments were performed using Genetic optimization for ligand docking (GOLD) program version 5.0.⁴⁸ All water molecules were removed and missing hydrogen atoms were added. The binding site is defined as a spherical region with a diameter of 12 Å and centered on the native ligand. Docking calculations were performed using Goldscore fitness function. The search efficiency was set as 90%.

4.6. CDOCKER docking procedure

Docking procedure was conducted by Discovery Studio (DS) v3.5 program.⁴⁹ All water molecules were removed. Missing hydrogen atoms were added at a pH of 7.0. The active site of the target protein was created as a spherical region with a diameter of 10 Å and centered on the FAD. Finally, the 10 top-ranking poses were saved for comparison and analysis.

4.7. Validation of the performance of molecular docking

Three different docking softwares were investigated, GOLD v5.0 (<http://gold.ccdc.cam.ac.uk/index.php>), Glide (standard precision) and CDOCKER. 56 reported LSD1 inhibitors were used for docking evaluation. 56, 51 and 39 molecules would be retrieved by Glide, Gold and CDOCKER tools, respectively. To further examine the merits, ROC analysis was performed. In general, the greater the AUC, the more effective the virtual screening workflow is in discriminating active from active compounds. For the test sets considered, standard precision (SP) of Glide outperformed GOLD, CDOCKER with ROC AUCs of 0.73.

4.8. In vitro LSD1 inhibition assay

The LSD1 screening biochemical assay was completed by and the detailed protocol was presented as followed. The LSD1 (Enzo Life Sciences) activity was monitored using the peroxidase-coupled assay system as described. Briefly, the compounds in DMSO were added into the LSD1 in the reaction buffer consisting of 50 mM Tris-HCl, pH 7.5, and 1% DMSO, by using Acoustic technology (Echo 550) in nanoliter range and incubated for 15 min at room temperature. The reactions were initiated by adding peptide substrate (10 μM Histone H3 (1–21) K4me2 peptide (AnaSpec)) to the reaction mixtures and incubated for 60 min at room temperature. The reactions were terminated by the addition of the detection mixture consisting final concentration of 0.1 Unit/ml horseradish peroxidase (Sigma) and 10 μM Amplex® UltraRed (Life Technologies) and fluorescence at $\text{Ex/Em} = 535/590$ nm was measured with kinetic mode of 5 min interval in Envision for 30 min. The signals after reaching plateau were taken for the data analysis. The background subtracted signals were calculated to % activities relative

to DMSO controls, and analyzed using GrapPad Prism 8 with “sigmoidal dose-response (variable slope)”; 4 parameters with Hill Slope.

4.9. MST experiment

The LSD1 recombinant from Millipore was labeled with a red fluorescent dye using a commercialized kit. The thermophoretic movement of the fluorescently labeled protein in complex with selected inhibitors was measured by monitoring the fluorescence distribution inside the capillary. The concentration of the labeled protein was kept constant at ~200 nM, while the concentration of the compound was varied. The samples were loaded into MST-grade glass capillaries. After a short incubation period, the MST analysis was performed using the Monolith NT.115.

4.10. MAO-A and MAO-B assays

The MAO-A and MAO-B is purchased from Active Motif (Cat#31502, Cat#31503). Biochemical Kit is purchased from Promega (MAO-Glo Assay, V1402). The inhibition of selectivity assay was performed in light of the manufacturer's protocol. Luminescence is read on Gen5 BioTek Spectrometer and data is processed using GraphPad Prism 8.

4.11. Reversibility assay

Using jump dilution analysis to determine the reversibility of compounds. Briefly, the compound **12a** at the concentrations of $10 \times$ their biochemical IC_{50} s were pre-incubated with high concentration of LSD1 protein (500 nM) for 1 h, and then diluted 100-fold by H3K4me2 peptide solution. The data was plotted in GraphPad Prism 8.

4.12. Flow cytometry assay

FACS analyses were performed using an LSR Model II flow cytometer (BD Biosciences, Oxford, UK). Cell sorting experiments were performed using either an Influx or a FACS Aria flow cytometer (both from BD Biosciences). CD11b antibody is purchased from BD.

4.13. Western blot assay

H3K4me1 antibody (Active Motif 39297), H3K4me2 (Millipore 07-030 (Crossreacting K4me1, should use 1:4000 above), H3K4me3 (CS 9751S (use 1:5000 above) antibodies are used in the western blot assay.

5. Declaration of interest

F. L. is a shareholder of Constellation Pharmaceuticals Inc. as well as a consultant of Active Motif. The other authors declare no competing financial interests.

Acknowledgments

X. Z. and Y. X. thank the financial support by the Natural Science Foundation of Jiangsu Province (BK20161458), “Six Talent Peaks” Project of Jiangsu Province (2016-YY-042), the Outstanding Scientific and Technological Innovation Team of Jiangsu Province of China

(2015) and the Priority Academic Program Development of Jiangsu Higher Education Institutions (PAPD). F. L. thanks the financial support by China “Thousand Youth Talents” Project (KHH1340001) and the National Natural Science Foundation of China (91419306).

Appendix A. Supplementary data

Supplementary data associated with this article can be found, in the online version, at <https://doi.org/10.1016/j.bmc.2018.08.026>.

References

- Shi YJ, Lan F, Matson C, et al. *Cell*. 2004;119:941–953.
- Dawson MA, Kouzarides T. *Cell*. 2012;150:12–27.
- Metzger E, Wissmann M, Yin N, et al. *Nature*. 2005;437:436–439.
- Lizcano F, Garcia J. *Pharmaceuticals*. 2012;5:963–990.
- Etani T, Suzuki T, Naiki T, et al. *Oncotarg*. 2015;6:2865–2878.
- Arrowsmith CH, Bountra C, Fish PV, Lee K, Schapira M. *Nat Rev Drug Discovery*. 2012;11:384–400.
- He Y, Korboukh I, Jin J, Huang J. *Acta Biochim Biophys Sin*. 2012;44:70–79.
- Jin L, Hanigan CL, Wu Y, Wang W, Park BH, et al. *Biochem J*. 2013;449:459–468.
- Amente S, Lania L, Majello B. *Biochim Biophys Acta, Gene Regul Mech*. 2013;1829:981–986.
- Harris WJ, Huang X, Lynch JT, et al. *Cancer Cell*. 2012;21:473–487.
- Schenk T, Chen WC, Gollner S, Howell L, Jin LQ, et al. *Nat Med*. 2012;18:605–611.
- Hayami S, Kelly JD, Cho HS, et al. *Int J Cancer*. 2011;128:574–586.
- Kauffman EC, Robinson BD, Downes MJ, et al. *Mol Carcinog*. 2011;50:931–944.
- Wang P, Fan F, Li X, et al. *J Mol Cell Cardiol*. 2018;115:115–129.
- Helin K, Dhanak D. *Nature*. 2013;502:480–488.
- Zheng YC, Ma J, Wang Z, Li J, Jiang B, et al. *Med. Res. Rev*. 2015;35:1032–1071.
- Stazi G, Zwergel C, Valente S, Mai A. *Expert Opin Ther Pat*. 2016;26:565–580.
- Mould DP, McGonagle AE, Wiseman DH, Williams EL, Jordan AM. *Med Res Rev*. 2015;35:586–618.
- Forneris F, Binda C, Battaglioli E, Mattevi A. *Trends Biochem Sci*. 2008;33:181–189.
- Ueda R, Suzuki T, Mino K, et al. *J Am Chem Soc*. 2009;131:17536–17537.
- Binda C, Valente S, Romanenghi S, et al. *J Am Chem Soc*. 2010;132:6827–6833.
- Valente S, Rodriguez V, Mercurio C, et al. *Eur J Med Chem*. 2015;94:163–174.
- Mimasu S, Sengoku T, Fukuzawa S, Umehara T, Yokoyama S. *Biochem Biophys Res Commun*. 2008;366:15–22.
- Mimasu S, Umezawa N, Sato S, Higuchi T, Umehara T, Yokoyama S. *Biochemistry*. 2010;49:6494–6503.
- Zheng YC, Yu B, Chen ZS, Liu Y, Liu HM. *Epigenomics*. 2016;8:651–666.
- Zheng YC, Yu B, Jiang GZ, et al. *Curr Top Med Chem*. 2016;16:2179–2188.
- Mohammad HP, Smitheman KN, Kamat CD, et al. *Cancer Cell*. 2015;28:57–69.
- Gallipoli P, Giotopoulos G, Huntly B. *J. Ther Adv Hematol*. 2015;6:103–119.
- Hoang N, Zhang X, Zhang C, et al. *Bioorg Med Chem*. 2018;26:1523–1537.
- Kumar V, Rosse G. *ACS Med Chem Lett*. 2016;7:132–133.
- Wu F, Zhou C, Yao Y, et al. *J Med Chem*. 2016;59:253–263.
- Nowotarski SL, Pachaiyappan B, Holshouser SL, et al. *Bioorg Med Chem*. 2015;23:1601–1612.
- Sartori L, Mercurio C, Amigoni F, et al. *J Med Chem*. 2017;60:1673–1692.
- Vianello P, Sartori L, Amigoni F, et al. *J Med Chem*. 2017;60:1693–1715.
- Young K, Lin S, Sun L, Lee E, Modi M, et al. *Nat Biotechnol*. 1998;16:946–950.
- Hamasaki K, Rando RR. *Anal Biochem*. 1998;261:183–190.
- Nussinov R, Wolfson HJ. *Comb Chem High Throughput Screening*. 1999;2:261–269.
- Olson AJ, Goodsell DS. *SAR QSAR Environ Res*. 1998;8:273–285.
- Hazeldine S, Pachaiyappan B, Steinbergs N, Nowotarski S, Hanson AS, et al. *J Med Chem*. 2012;55:7378–7391.
- Zha XM, Wu LM, Xu SY, et al. *Med Chem Res*. 2016;25:2822–2831.
- Zhou C, Kang D, Xu YG, Zhang LY, Zha XM. *Chem Biol Drug Des*. 2015;85:659–671.
- Xi JY, Xu SY, Wu LM, Ma TF, et al. *Bioorg Chem*. 2017;72:182–189.
- In Kurzer F. *Organic Synthesis*. Wiley: New-York. 1964;4:49–50.
- Lanotte M, Martin-Thouvenin V, Najman S, Balerini P, Valensi F, Berger R. *Blood*. 1991;77:1080–1086.
- Lee HT, Choi MR, Doh MS, Jung KH, Chai YG. *Oncol Rep*. 2013;30:1587–1592.
- Rivers A, Vaitkus K, Ruiz MA, Ibanez V, et al. *Exp Hematol*. 2015;43:546–553.
- Liu TX, Zhang JW, Tao J, Zhang RB, Zhang QH, et al. *Blood*. 2000;96:1496–1504.
- Mackey MD, Melville JL. *J Chem Inf Model*. 2009;49:1154–1162.
- Konagurthas AS, Whisstock JC, Stuckey PJ, Lesk AM. *Proteins*. 2006;64:559–574.